# Multifractality and chaos in the solar wind

Wiesław M. Macek

*Faculty of Mathematics and Natural Sciences, School of Exact Sciences,*
*Cardinal Stefan Wyszyński Uniwersity in Warsaw, Dewajtis 5, 00-815 Warszawa;*
*Space Research Centre, Polish Academy of Sciences, Bartycka 18 A, 00-716 Warszawa, Poland*

**Abstract.** We analyze a time series of velocities of the solar wind plasma stream including Alfvénic fluctuations measured *in situ* by the Helios spacecraft in the inner heliosphere, which is the region of space dominated by the solar wind flow. We calculate the generalized dimensions directly from the cleaned experimental signal. The resulting spectrum of dimensions shows multifractal structure of the solar wind in the inner heliosphere. The obtained multifractal spectrum is consistent with that for the multifractal measure on the self-similar weighted Cantor set.

The generalized dimensions of attractors are important characteristics of *complex* dynamical systems [1]. Since these dimensions are related to frequencies with which typical orbits in phase space visit different regions of the attractors, they provide information about dynamics of the systems [2, 3]. More precisely, one may distinguish a probability measure from its geometrical support, which may or may not have fractal geometry. Then, if the measure has different fractal dimensions on different parts of the support, the measure is multifractal [4, 5]. The modern technique of nonlinear time series analysis allows to estimate the multifractal measure directly from a single time series.

Following space physics applications, e.g., [6, 7], we consider the inner heliosphere. Since the 1960s we have known that besides electromagnetic radiation, the Sun also radiates charged particles forming a plasma blowing nearly radially outward from the Sun. The solar wind plasma flowing supersonically away from the Sun is quite well modeled within the framework of the hydromagnetic theory. This continuous flow has two forms: slow ($\approx 300$ km s$^{-1}$) and fast ($\approx 900$ km s$^{-1}$) [8]. The fast wind is associated with coronal holes and is relatively uniform and stable, while the slow wind is quite variable in terms of velocities. We limit our study to the low-speed stream. Indication for a chaotic attractor in the slow solar wind has recently been given in [9, 10, 11, 12, 13]. In particular, Macek [9, 10] has calculated the correlation dimension of the reconstructed attractor and has provided tests for *nonlinearity* in the solar wind data, including a powerful method of singular-value decomposition [14] and statistical surrogate data tests [15]. Further, Macek and Redaelli [13] have shown that the Kolmogorov entropy of the attractor is *positive* and finite, as it holds for a *chaotic* system. The entropy is plausibly constrained by a *positive* local Lyapunov exponent that would exhibit sensitive dependence on initial conditions of the system.

In the present paper we have extended our previous results on the dimensional time series analysis [9]. Namely, we apply the technique that allows a realistic calculation of the generalized dimensions of the solar wind flow, directly from the cleaned experimental signal by using the Grassberger and Procaccia method [16]. The resulting spectrum

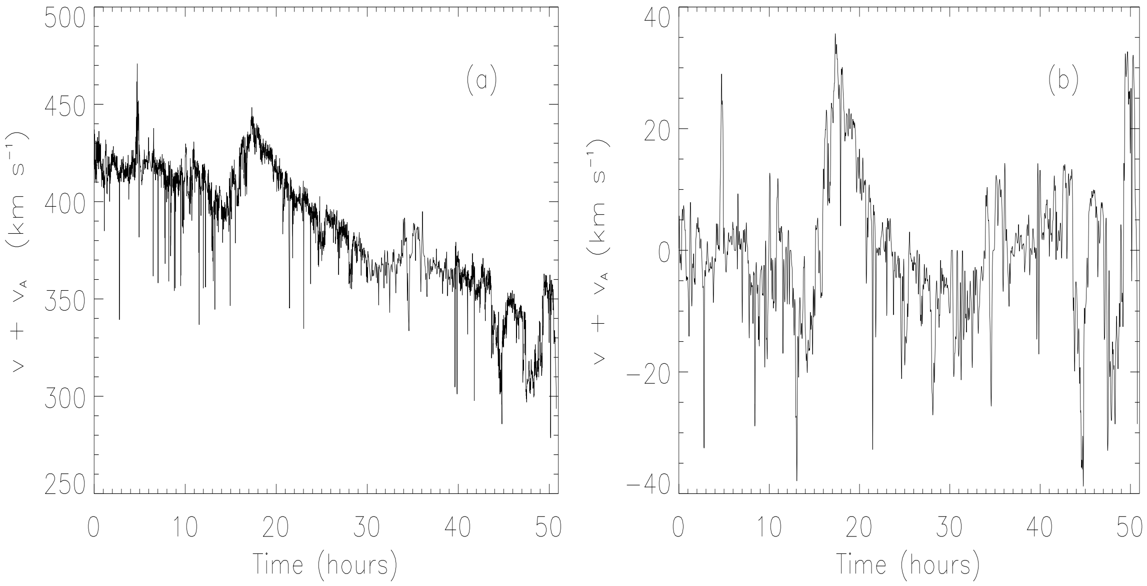


**FIGURE 1.** The flow velocity with included Alfvénic velocity, $v+v_A$ (Elssäser variable) observed by the Helios 1 spacecraft in 1975 from 67:08:20.5 to 69:11:07 (day:h:min) at distances 0.32 AU from the Sun, (a) the raw data, (b) the detrended and smoothed data.

of dimensions shows multifractal structure of the solar wind in the inner heliosphere. The obtained multifractal spectrum is consistent with that for the multifractal measure on the self-similar weighted Cantor set, e.g., [5].

These results provide supporting evidence that the *complex* solar wind is likely to have multifractal structure, cf. [7]. In this way, we have further supported our previous conjecture that trajectories describing the system in the inertial manifold of phase space asymptotically approach the attractor of low-dimension [9, 10, 13]. One can expect that the attractor in the low-speed solar wind plasma should contain information about the dynamic variations of the coronal streamers. It is also possible that it represents a structure of the time sequence of near-Sun coronal fine-stream tubes.

We analyze the Helios data using plasma parameters measured *in situ* in the heliosphere near the Sun, at 0.3 AU, Ref. [8]. The radial velocity component of the plasma flow, $v$, has been investigated in [9, 10, 13]. However, it is known that various disturbances are superimposed on the overall structure of the solar wind, including mainly Alfvén waves, which move away from the Sun. Therefore, in this paper we take also into account Alfvénic fluctuations of the flow. Namely, we analyze one of the so-called Elssäser variables $x=v+v_A$, where $v_A = B/(\mu_o \rho)^{1/2}$ is the Alfvénic velocity calculated from the experimental data: the radial component of the magnetic field of the plasma $B$ and the mass density $\rho$ ($\mu_o$ is the permeability of free space). These raw data of $N=4,513$ points, with sampling time of $\Delta t = 40.5$ s, are shown in Figure 1 (a).

As in [9, 13], slow trends ($420.06 - 15.4\ t - 82.31\ t^2$, with $t$ being a fraction of total sample) were subtracted from the original data $x_i = v(t_i) + v_A(t_i)$, in km s$^{-1}$, $i = 1,\ldots,N$ and the data with the initial several percent noise level, were (8-fold) smoothed (replacing each data point with the average of itself and its two nearest

**TABLE 1.** Characteristics of the solar wind, $v + v_A$, filtered data.

| | Smoothed | Shuffled data | Shuffled phases |
|---|---|---|---|
| Skewness, $\kappa_3$ | 0.26 | 0.26 | -0.26 |
| Kurtosis, $\kappa_4$ | 0.88 | 0.88 | 0.26 |
| Relative complexity | 0.17 | 1.0 | 0.23 |
| Autocorrelation time, $t_a$ | $3.5 \times 10^3$ s | 40 s | $3.3 \times 10^3$ s |
| Capacity dimension, $D_0$ | 4.4 | 5.8 | 4.6 |
| Information dimension, $D_1$ | 4.0 | 5.0 | 4.5 |
| Correlation dimension, $D_2$* | 3.5 | 5.2 | 4.6 |

* The average slope for $6 \leq m \leq 8$ is taken as $D_2$.

neighbors). The detrended and smoothed data shown in Figure 1 (b). Certainly, this moving average filter removes considerable amount of noise, leaving only about 1%. The nonlinear filtering, which allows calculation of the entropy, has been discussed in [13]. It has been shown that after the nonlinear Schreiber filter the calculated dimension has been somewhat reduced. In this paper, we focus on the calculations of dimensions. Therefore, we prefer to use only moving average filtering, cf. [9]. It is worth noting that our solar wind data in Figure 1 (b) resemble somewhat the time series in Figure 2 of Ref. [4], which is a simulation of a sample from a multifractal measure.

Table 1 summarizes selected calculated characteristics of the detrended data cleaned by using the moving average filter. The probability distributions are clearly non-Gaussian, cf. Ref [13]. We have a large skewness of $\sim 0.26$ (as compared with its normal standard deviation 0.06) and a very large kurtosis of 0.88 (the latter was small for the analysis with no magnetic field), cf. Ref [9]. We have also estimated Lempel-Ziv measure of *complexity*, relative to white noise [17]. The calculated value $\sim 0.17$ is even smaller than in [9] ($\approx 0.20$); maximal complexity, or randomness, would have a value of 1.0, while a value of zero denotes perfect deterministic nonlinear predictability. We choose a time delay $\tau = 150\ \Delta t$, where the autocorrelation function has the first minimum and its value is very small. This value is smaller than $t_0 = 376\ \Delta t$, the first zero of the autocorrelation function, $(\langle x(t)x(t+t_0)\rangle - \langle x(t)\rangle^2)/\sigma^2 = 0$ with average velocity $\langle x \rangle = -0.36$ km s$^{-1}$ and standard deviation $\sigma = 8.54$ km s$^{-1}$, cf. also $t_a$ in Table 1 when the autocorrelation function decreases to $1/e$.

Using our time series of equally spaced, detrended and cleaned data, we construct a large number of vectors $\mathbf{X}(t_i) = [x(t_i), x(t_i+\tau), \ldots, x(t_i+(m-1)\tau)]$ in the embedding phase space of dimension $m$, where $i = 1, \ldots, n$ with $n = N-(m-1)\tau$. Then, we divide this space into a large number $M(r)$ of equal hypercubes of size $r$ which cover the presumed attractor. If $p_j$ is the probability measure that a point from a time series falls in a typical $j$-th hypercube, using the $q$-order function $I_q(r) = \sum(p_j)^q$, $j = 1, \ldots, M$, the $q$-order generalized dimension is given by [2, 3]

$$D_q = \frac{1}{q-1} \lim_{r \to 0} \frac{\ln I_q(r)}{\ln r} \ , \tag{1}$$

We see from Eq. (1) that the larger $q$ is, the more strongly are the higher probability cubes (visited more frequently by a trajectory) weighted in the sum for $I_q(r)$. Only if $q = 0$, all the cubes are counted equally, $I_o = M$, and we recover the box-counting dimension, $D_0$.

Writing $I_q(r) = \sum p_j(p_j)^{q-1}$ as a weighted average $\langle(p_j)^{q-1}\rangle$, one can associate bulk with the generalized average probability per hypercube $\mu = \sqrt[q-1]{\langle(p_j)^{q-1}\rangle}$, and identify $D_q$ as a scaling of bulk with size, $\mu \propto r^{D_q}$. Since the data cannot constrain well the capacity dimension $D_0$, we look for higher order dimensions, which quantify the multifractality of the probability measure on the attractor. For example, the limit $q \to 1$ leads to a geometrical average (the information dimension). For $q = 2$ the generalized average is the ordinary arithmetic average (the standard correlation dimension), and for $q = 3$ it is a root-mean-square average. In practice, for a given $m$ and $r$,

$$p_j \simeq \frac{1}{n - 2n_{\rm c} - 1} \sum_{i=n_c+1}^{n} \theta(r- \mid \mathbf{X}(t_i) - \mathbf{X}(t_j) \mid) \tag{2}$$

with $\theta(x)$ being the unit step function, and $n_{\rm c} = 2$ is the Theiler's correction [19]. Finally, $I_q(r)$ is taken to be equal to the generalized $q$-point correlation sum [16]

$$C_q(m,r) \;=\; \frac{1}{n_{\rm ref}} \sum_{j=1}^{n_{\rm ref}} (p_j)^{q-1}, \tag{3}$$

where $n_{\rm ref} = 500$ is the number of reference vectors. For large dimensions $m$ and small distances $r$ in the scaling region it can be argued that $C_q(m,r) \propto r^{(q-1)D_q}$, where $D_q$ is an approximation of the ideal limit $r \to 0$ in Eq. (1) for a given $q$, Ref. [16].

First, we calculate the natural logarithm of the standard ($q = 2$) correlation sum $C_m(r) = C_2(m,r)$ versus $\ln r$ (normalized) for various embedding dimensions: $m = 4$ (dotted curve), $m = 5$ (diamonds), 6 (triangles), 7 (squares), 8 (crosses), 9 (plus), and 10 (stars) signs. The results obtained using the moving average filter are presented in Figure 2, while those obtained using the singular-value decomposition and nonlinear Schreiber filters have been discussed in [9, 10, 13]. The slopes $D_{2,m}(r) = \mathrm{d}[\ln C_m(r)]/\mathrm{d}(\ln r)$ in the scaling region of $r$ should provide the correlated dimension. Since the correlation sum is simply an arithmetic average over the numbers of neighbors, this can yield meaningful results for the dimension even when the number of neighbors available for some reference points is limited in most real dynamical systems. If the $D$-dimensional attractor exists, we expect a plateau of the slopes for $m \geq D$ and in the worst case for $m > 2D$. For $m$ large enough an average slope in the scaling region indicates a proper correlation dimension $D_2$. We have a clear plateau which appears already for $m = 4$ (dotted curve) and $m = 5$. For higher dimensions, $m \geq 8$, the plateau is still present but more smeared out by the statistical fluctuations at small $r$. In our case the slope of the calculated correlation sum saturates for $m > 5$, with an average for $6 \leq m \leq 8$ of $D_2 = 3.5 \pm 0.1$, cf. Ref. [9]; this is consistent with the attractor of the low-dimension.

Second, the generalized dimensions $D_q$ in Eq. (1) as a function of $q$ are shown in Figure 3. The error bars are purely statistical here. The spectrum of dimensions shows multifractal structure of the solar wind in the inner heliosphere. For comparison, the values calculated numerically for the standard Lorenz equations, using 2000 points at intervals of $\Delta t = 0.05$, $\tau = 5\,\Delta t$, are shown by plus signs. An extremely simple example of the multifractal system is the weighted Cantor set, where the probability of visiting one segment is $p$ (say $p \leq 1/2$) and the probability of visiting the other segment is $1 - p$.

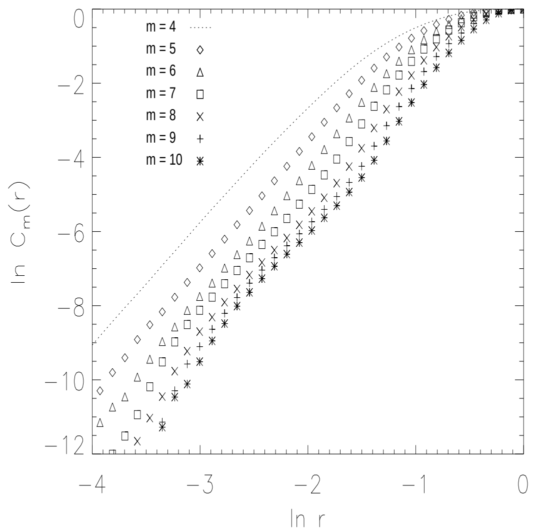


**FIGURE 2.** The natural logarithm of the correlation sum $C_m(r)$ versus $\ln r$ (normalized) obtained for the cleaned experimental signal for various embedding dimensions: $m = 4$ (dotted curve), $m = 5$ (diamonds), 6 (triangles), 7 (squares), 8 (crosses), 9 (plus), and 10 (stars).

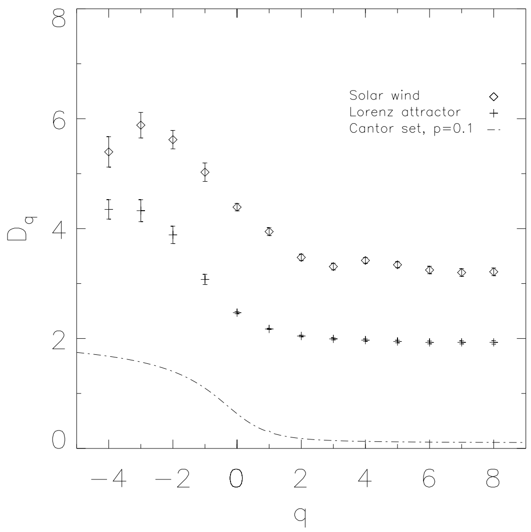


**FIGURE 3.** The generalized dimensions $D_q$ in Eq. (1) as a function of $q$. The correlation dimension is $D_2 = 3.5 \pm 0.1$, see Table 1. The values calculated numerically for the Lorenz model (plus signs) and analytically for the weighted Cantor set with $p = 0.1$ (dash-dotted).

In this case the results can be obtained analytically; for any $q$ in Eq. (1) one has

$$(1-q)D_q = log_3[p^q + (1-p)^q]. \tag{4}$$

The difference of the maximum and minimum dimension, associated with the least dense and most dense points on the attractor, correspondingly, is $D_{-\infty} - D_{\infty} = log_3(1/p - 1)$ and in the limit $p \to 0$ this difference rises to infinity. Hence, the parameter $p$ can be regarded as a degree of multifractality. The results calculated for $p = 0.1$ in Eq. (4) are shown in Figure 3 by a dash-dotted line. We see that the multifractal spectrum of the solar wind ($D_q - 3$) is roughly consistent with that for the multifractal measure on the self-similar weighted Cantor set, with a single weighting parameter $p$. The obtained value of this parameter demonstrates that some cubes that cover the attractor of this dynamical system are visited one order of magnitudes more frequently than some other cubes, as is illustrated in our previous paper, see Figure 5 of Ref. [9].

We also estimate the Kolmogorov correlation entropy, $K_2$, and the largest positive Lyapunov exponent, $\lambda_{\max}$. The vertical spacings between the parallel lines in Figure 2 averaged in the saturation region $8 \leq m \leq 10$ are taken as $K_2$ yielding the value of $\approx 0.1$ (per delay time $\tau$). Using the algorithm of Ref. [20], one obtains the magnitude of $\lambda_{\max} \sim 0.1$ in the same units as for $K_2$ (base e). In general, the entropy $K_q$ is at most the sum of the positive Lyapunov exponents $\sum \lambda_i$, e.g., [2, 3]. The value of the Lyapunov exponent is consistent with the Kolmogorov ($q = 2$) entropy, which should be its lower bound: $K_2 \leq \sum \lambda_i$ (positive). The time over which the meaningful prediction of the behavior of the system is possible is roughly $\sim 1/\lambda_{\max}$, e.g., [2, 3]. Hence the predictability of the system is limited to hours.

The obtained measures of the attractor have been subjected to the surrogate data test [15]. As has been demonstrated in Figure 8 of Ref. [9], if the original data are indeed deterministic, analysis of these surrogate data will provide values that are statistically distinct from those derived for the original data, see also Table 1. In particular, the slope of the correlation sum increases with $m$ (no saturation), and Lempel-Ziv complexity calculated for shuffled-data becomes clearly 1.0, as it should be for a purely stochastic system. Again, we have found that the solar wind data are sensitive to this test.

In conclusion, we have shown that the moving average filter removes some amount of noise, which is sufficient to calculate the generalized dimensions of the solar wind attractor. The obtained multifractal spectrum is consistent with that for the multifractal measure on the self-similar weighted Cantor set with a degree of multifractality of $p \sim 0.1$. The obtained characteristics of the attractor are significantly different from those of the surrogate data. Thus these results show multifractal structure of the solar wind in the inner heliosphere. Hence we suggest that there exists an inertial manifold for the solar wind, in which the system has *multifractal* structure, and where noise is certainly not dominant.

This work was supported by the Scientific Research Committee Grant 2 P03C 001 16.

## REFERENCES

1. Hentschel, H. G. E., and Procaccia, I., Physica D, **8**, 435–444 (1983); Grassberger, P., Phys. Lett. A, **97**, 227–230 (1983); Halsey, T. C., Jensen, M. H., Kadanoff, L. P., Procaccia, I., and Shraiman, B. I., Phys. Rev. A, **33**, 1141–1151 (1986).
2. Ott, E., *Chaos in Dynamical Systems*, Cambridge University Press, Cambridge, 1993.
3. Ott, E., Sauer, T., and Yorke, J. A., *Coping with Chaos*, Wiley, New York, 1994.
4. Mandelbrot, B. B., Multifractal measures, especially for the geophysicist, in *Pure and Applied Geophysics*, **131**, 5–42, Birkhäuser Verlag, Basel (1989).
5. Falconer, K., *Fractal Geometry: Mathematical Foundations and Applications*, Wiley, New York, 1990.
6. Kurths, J., and Herzel, H., Physica D, **25**, 165–172 (1987).
7. Burlaga, L. F., Geophys. Res. Lett., **18**, 69–72 (1991).
8. Schwenn, R., Large-scale structure of the interplanetary medium, in *Physics of the Inner Heliosphere*, edited by R. Schwenn and E. Marsch, Springer-Verlag, Berlin, 1990, Vol. 20, pp. 99–182.
9. Macek, W. M., Physica D, **122**, 254–264 (1998).
10. Macek, W. M., Testing for an attractor in the low-speed solar wind flow, in *Solar Wind Nine*, edited by S. R. Habbal, R. Esser, J. V. Hollweg, and P. A. Isenberg, American Institute of Physics, New York, 1999, Vol. 471, pp. 251–254.
11. Macek, W. M., and Obojska, L., Fractal analysis of the low-speed solar wind flow, in ESA Symposium Proceedings on *Environment Modelling for Space-based Applications*, edited by A. Hilgers and T. -D. Guyenne, ESTEC, Noordwijk, 1996, *SP-392*, pp. 247–252.
12. Macek W. M., and Obojska, L., Chaos, Solitons & Fractals, **8**, 1601–1607 (1997); **9**, 221–229 (1998).
13. Macek W. M., and Redaelli, S., Phys. Rev. E, **62**, 6496–6501 (2000).
14. Albano, A. M., Muench, J., Schwartz, C., Mees, A. I., and Rapp, P. E., Phys. Rev. A, **38**, 3017–3026 (1988).
15. Theiler, J., Eubank, S., Longtin, A., Galdrikian, B., and Farmer, J. D., Physica D, **58**, 77–94 (1992).
16. Grassberger P., and Procaccia, I. , Physica D, **9**, 189–208 (1983).
17. Kaspar, F., and Schuster, H. G., Phys. Rev. A, **36**, 842–848 (1987).
18. Grassberger P., and Procaccia, I., Phys. Rev. A, **28**, 2591–2593 (1983).
19. Theiler, J., Phys. Rev. A, **34**, 2427–2432 (1986).
20. Kantz, H., Phys. Lett. A, **185**, 77–87 (1994).